International Journal of Clinical & Medical Informatics

ISSN: 2582-2268 Review Article | Vol 5 Iss 1

Tunable Plasmonic Band-Pass Filter Using Five Circular Ring Resonators

Hamid Abbasi

University of Mazandaran, Iran

Correspondence should be addressed to Hamid Abbasi, University of Mazandaran, Iran

Received: March 11, 2022; Accepted: March 24, 2022; Published: March 31, 2022

ABSTRACT

This paper investigates and builds a highly sensitive refractive index sensor based on the resonance system in plasmonic structure. The proposed sensor structure consists of two waveguides and five loops. The results show that the resonance wavelength changes significantly with increasing refractive index, which proves that this method is suitable for understanding and analyzing the behavior of resonance wavelength and refractive index. In this research, we examine the characteristics of measurement such as sensitivity and quality factor and competency form (FOM). Compared to replicon sensors based on a similar structure, this proposed sensor can accept a more flexible amplitude of wavelength and a wider range of refractive index. As a result of this approach, it can be used in areas such as biochemical and medical analysis.

KEYWORDS

Photonics; Plasmonics; Surface plasmons; Waveguides; Resonators; Optics

INTRODUCTION

Researchers have begun to compress plasmonic structures to make them easier to use, given the functional and important properties of optical circuits and their increased use. These structures consist of metal and dielectric. Plasmonic science means enclosing electromagnetic waves in dimensions much smaller than the radiant wavelength. Plasmonic science can also be found in the interaction of radiant electromagnetic waves on the surface of metals and their conducting electrons. Plasmonic has two parts: localized superficial plasmons and superficial polariton plasmons. Surface plasmon resonance (SPR) can generate a strong electromagnetic field enhancement on the surface of a metal structure, and is very sensitive to the surrounding environment.

Therefore, SPR can be applied to numerous fields such as absorption enhancement [1,2], magnetic field enhancement [3,4], photocatalysis [5-10], THz oscillation [11-13], Fano resonance [14-17], surface -enhanced Raman scattering (SERS) [18-21], subwavelength lithography [22,23], and refractive index (RI) sensors [24-29]. For refractive index sensors based on SPR, the resonance is excited mainly in two modes, the angular mode (at fixed wavelength) and the spectral mode (at fixed angle) [30,31]. In this research, we turn to the second mode, the spectral mode, because due to the low efficiency of the first mode (angular) in a real system, the wavelength scanning method is preferred as a better and faster tool for measuring the reflection spectrum. Plasmonic filters based on MIM waveguide structures, such as asymmetric nanodisk filters and sensors [32-34], circular ring filters and sensors [35,36], lateral coupled cavity

Citation: Hamid Abbasi, Tunable Plasmonic Band-Pass Filter Using Five Circular Ring Resonators. Int J Clin Med Info 5(1): 26-32.

sensors [37] as well as cut-off intensifier sensors [38], Is one of the most important and practical optical devices that have attracted much attention.To build plasmonic sensors, parameters such as high transmission efficiency, high quality factor, high resolution, optical stability, sensitivity enhancement and adjustability in a range of wavelengths must be considered. By analyzing and increasing the quality of these parameters, we can help increase the speed of information processing in optically integrated circuits. By analyzing and reviewing and increasing the quality of these parameters, we can help increase the speed of information processing in optically integrated circuits. In this paper, a wavelength change filter consisting of two waveguides and circular amplifiers is proposed and investigated. To analyze this proposal, numerical simulation will be performed using the finite difference method of time domain, but the related diagrams will be drawn in MATLAB software.

STRUCTURAL MODEL AND THEORY ANALYSIS

The basic equations resulting from the interaction of electromagnetic waves and matter are expressed by Maxwell's equationsIn a frequency range, the optical properties of metals are explained by a plasma model, the Drud model. Electrons will oscillate in response to the applied electromagnetic field. In the free electron model, at frequencies much larger than the plasma frequency, the dielectric function tends to zero. For noble metals, generalization of this model to a frequency range greater than the plasma frequency creates a highly polar environment due to the filling of the band close to the Fermi surface [39]. The simulation using

the time domain finite difference method with the Drude model for real for real metals is as follows [40]:

$$\varepsilon(\omega) = \varepsilon_\infty - \omega_p^2 / \omega^2 + i\Upsilon\omega \quad (1)$$

Here $\varepsilon\infty = 1$ gives the medium constant for the infinite frequency, $\gamma = 3.21 \times 1013$ means damping frequency for electron oscillation, $\omega p = 1.37 \times 1016$ refers to bulk frequency for plasma and ω shows incident light angular frequency. The structure of the sensor, which consists of two waveguides and five rings, is shown in Figure 1. The width of the two waveguides is w = 50 nm. The middle ring has an inner radius of r1 = 97 nm and an outer radius of R1 = 140 nm and its distance from the waveguides is 12 nm. The 4 upper and lower rings have an inner radius of r2 = 110 nm and an outer radius of R2 = 150 nm. Pin and Pout are monitors that measure the input wave and the output wave, respectively, by calculating the natural component of the Poin Ting vector along the blurred lines. The transfer is calculated by the following equation:

$$T = Pout / Pin \quad (2)$$

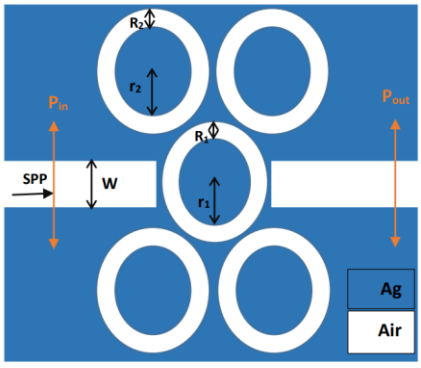

Figure 1: Two-dimensional image of a plasmonic sensor.

We consider the environment inside the rings and waveguides as air and the simulation bed as silver. To distribute the field in the sensor structure, we enter the input wave from the left into the sensor structure. The wave goes to the output after passing through the resonators. Each resonator will reflect some input wax. To achieve the maximum field distribution in the simulated structure, all dimensions must be optimized, otherwise we must change the dimensions of the structure to achieve the maximum field distribution (Figure 2).

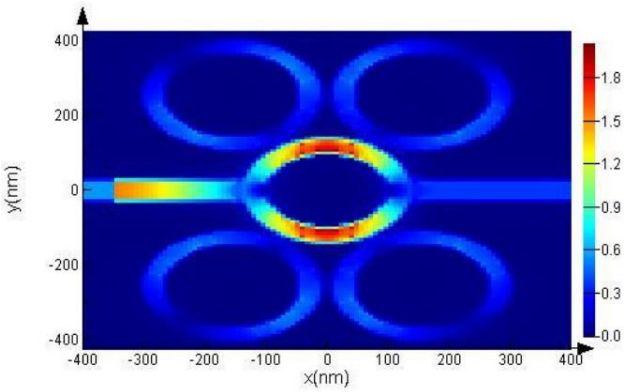

Figure 2: Plasmonic sensor field distribution.

FRACTURE COEFFICIENT SIMULATION AND MEASUREMENT METHODS

The proposed plasmonic resonance behavior is investigated numerically and theoretically. For the numerical approach, we use the finite difference method of the time domain with 8 layers completely compatible with the absorption of boundary conditions. The mesh size for both x and y directions is 8 nanometers. To reduce the simulation time and improve the performance of the plasmonic sensor, we will perform the simulation in two dimensions, and then to investigate the spectral responses of the proposed structure, we will obtain the waveguide transmission spectra (Fig.3). To do this, we increase the refractive index of the middle ring by a step of 0.01 from 1.15 to 1.2 and the refractive index of other rings and waveguides remains constant. This changes the resonance spectra and wavelengths. The sensor transmission spectrum has three peaks that the right peak (in the range of 1300-1600 wavelength) has more wavelength change than the other two peaks and has more flexibility in changing the refractive index and wavelength shift. So it will provide better performance. We conclude that in the design of sensors, the amount of change in resonance wavelength is more important than the height of the peaks.

To measure the performance of a plasmonic sensor, we need to calculate a few important factors so that we can make an acceptable and quality sensor.

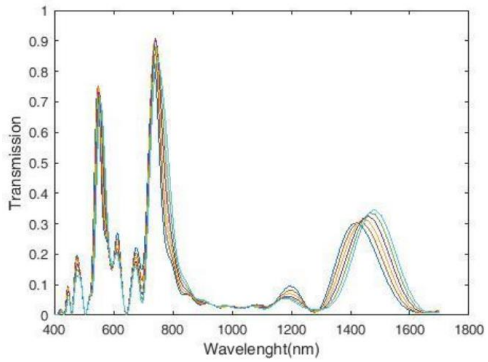

Figure 3: Transmission spectra of a plasmonic refractive index with two cavities.

The first and most attractive performance feature for plasmonic sensors is the detection of the S sensitivity coefficient, which is explained by the following equation:

$$S = \Delta \lambda / \Delta n \text{ (nm/RIU)} \quad (3)$$

Here Δn is the refractive index change and λres is the wavelength at which SP is excited. Depending on the resonant wavelength, geometry of the structure and properties of the simulation substrate, the sensitivity can vary considerably. According to Figure 4, the maximum sensitivity for the refractive index is n = 1.2 (mode 3), which is equal to 2081 nm / RIU. According to Equation 3 and the diagrams in Figure 4, the resonance wave gradually shifts and its slope increases with increasing refractive index. So there is a linear relationship between the refractive index and the resonant wavelength.

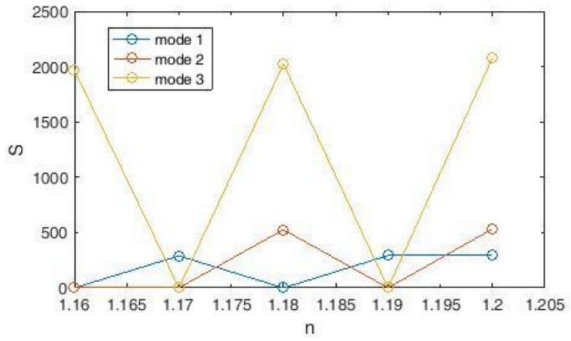

Figure 4: Plasmonic sensor sensitivity coefficient diagram.

By plotting the field distribution shape for the state with the most sensitivity coefficient (2081 nm / RIU sensitivity coefficient for the refractive index n = 1.2 (mode 3)), we conclude that, as in the initial state, the maximum wave value and the resulting field will go to the middle ring, but the 4 surrounding rings will have more field distribution than the initial state and will have a greater share in measuring the sensor (Figure 5).

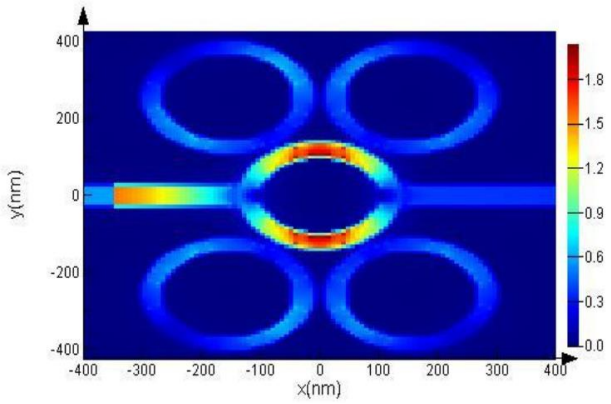

Figure 5: Electric field distribution at resonant frequency.

The sensitivity coefficient S is directly related to the ability of the plasmonic sensor to measure small changes in the refractive index. Therefore, a combination of these parameters will be known as the figure of merit (FOM). FOM is widely used to compare and evaluate different sensors according to their sensory point of view and is expressed as the following equation:

$$FOM = S / FWHM \quad (4)$$

We see the figure of merit (FOM) of the designed sensor in Figure 6. The maximum value of FOM is for refractive index n = 1.2 (mode 3), which is equal to 12.8639 nm / RIU.

The third factor to evaluate the sensor is the quality factor Q:

$$Q = \lambda res / FWHM \quad (5)$$

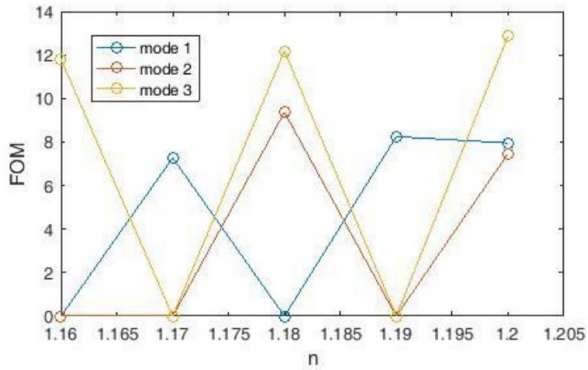

Figure 6: Plasmonic sensor figure of merit (FOM) diagram.

We see the diagram of the quality coefficient of the plasmonic sensor in Figure 7. The maximum quality coefficient for the refractive index is n = 1.16 (mode 1), which is equal to 18.866 nm/RIU.

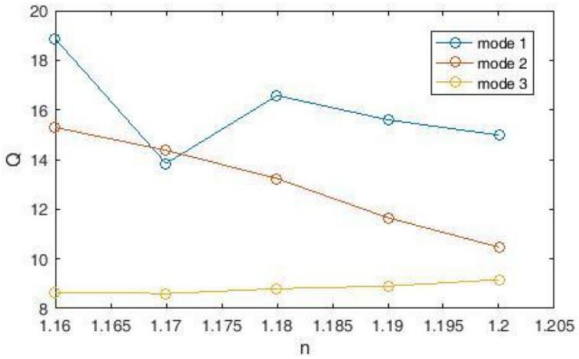

Figure 7: Q coefficient diagram of Q plasmonic sensor.

Using Equations 3, 4 and 5, we draw the graphs of coefficient of sensitivity, coefficient of quality and figure of merit (FOM).

CONCLUSION

Recent advances in plasmonic nanostructure technologies have prompted researchers to discover plasmonic sensors. Various plasmonic modes such as surface plasmon polarities (SPPs), localized surface plasmons (LSPs), associated LSP-PSP modes, and surface lattice resonances supported by metal or metal-dielectric-metal structures for detection and marking. Giving attractive technology features are introduced. This study focuses mainly on plasmonic waveguides, fabrication techniques and

navigation methods. In general, any plasmonic waveguide will show a trade-off between loss of propagation and absorption of diffusion. Using this information and designing a suitable structure for our desired sensor, we have reached a sensitivity coefficient above 2081 nm / RIU. With increasing discoveries based on surface plasmon wave conduction in subwave or deep wavelength regimes, the plasmonic field is expected to dominate the research and development of integrated optical communications, data storage, optical sensing, and imaging technology.

REFERENCES

1. Cen CL, Liu L, Zhang YB, et al. (2019) Tunable absorption enhancement in periodic elliptical hollow graphene arrays. Optical Materials Express 9(2): 706-716.
2. Lin H, Ye X, Chen XF, et al. (2019) Plasmonic absorption enhancement in grapheme circular and elliptical disk arrays. Materials Research Express 6(4): 045807.
3. Chen J, Zhang T, Tang CJ, et al. (2016) Optical magnetic field enhancement via coupling magnetic plasmons to optical cavity modes. IEEE Photonics Technology Letters 28(14): 1529-1532.
4. Chen J, Tang CJ, Mao P, et al. (2016) Surface-plasmonpolaritons-assisted enhanced magnetic response at optical frequencies in metamaterials. IEEE Photonics Journal 8(1): 4800107.
5. Hou WB, Cronin SBA (2013) A review of surface plasmon resonance enhanced photocatalysis. Advanced Functional Materials 23(13): 1612-1619.
6. Zhao XX, Yang H, Li SH, et al. (2018) Synthesis and theoretical study of large-sized Bi4Ti3O12 square nanosheets with high photocatalytic activity. Materials Research Bulletin 107: 180-188.
7. Di LJ, Yang H, Xian T, et al. (2018) Construction of Z-scheme g-C3N4/CNT/Bi2Fe4O9 composites with improved simulated-sunlight photocatalytic activity for the dye degradation. Micromachines 9(12): 613.
8. Yan YX, Yang H, Zhao XX, et al. (2018) Enhanced photocatalytic activity of surface disorder-engineered CaTiO3. Materials Research Bulletin 105: 286-290.
9. Zheng CX, Yang H, Cui ZM, et al. (2017) A novel Bi4Ti3O12/Ag3PO4 heterojunction photocatalyst with enhanced photocatalytic performance. Nanoscale Research Letters 12: 608.
10. Di LJ, Yang H, Xian T, et al. (2018) Facile synthesis and enhanced visible-light photocatalytic activity of novel p-Ag3PO4/n BiFeO3 heterojunction composites for dye degradation. Nanoscale Research Letters 13: 257.
11. Safaria S, Jazi B (2017) The role of terahertz surface plasmons in the scattering pattern of electromagnetic waves in an unstable elliptical plasma antenna. Physics of Plasmas 24: 072112.
12. Du HM, Zhang LP, Li DA (2018) THz plasma wave instability in field effect transistor with electron diffusion current density. Plasma Science and Technology 20(11): 115001.
13. Li DG, Zhang LP, Du HM (2019) The instability of terahertz plasma waves in cylindrical FET. Plasma Science and Technology 21(4): 045002.
14. Wang JC, Song C, Hang J, et al. (2017) Tunable Fano resonance based on grating-coupled and graphene-based Otto configuration. Optics Express 25: 23880-23892.
15. Zhang XW, Qi YP, Zhou PY, et al. (2018) Refractive index sensor based on fano resonances in plasmonic waveguide with dual side-coupled ring resonators. Photonic Sensor 8(4): 367-374.

16. Piao XJ, Yu S, Koo S, et al. (2011) Fano-type spectral asymmetry and its control for plasmonic metal-insulator-metal stub structures. Optics Express 19(11): 10907-10912.
17. Piao XJ, Yu S, Park N (2012) Control of Fano asymmetry in plasmon induced transparency and its application to plasmonic waveguide modulator. Optics Express 20: 18994-18999.
18. Liu GQ, Yu MD, Liu ZQ, et al. (2015) One-process fabrication of metal hierarchical nanostructures with rich nanogaps for highly-sensitive surface-enhanced Raman scattering. Nanotechnology 26: 185702.
19. Wang XX, Bai XL, Pang ZY, et al. (2019) Surface-enhanced Raman scattering effect of a composite structure with gold nano-cubes and gold film separated by Polymethylmethacrylate film. Acta Phys. Sin 68(3): 037301.
20. Yu MD, Huang ZP, Liu ZQ, et al. (2018) Annealed gold nanoshells with highly-dense hotspots for large-area efficient Raman scattering substrates. Sensors and Actuators B: Chemical 262: 845-851.
21. Wang XX, Bai XL, Pang ZY, et al. (2019) Investigation of surface plasmons in Kretschmann structure loaded with a silver nano cube. Results in Physics 12: 1866-1870.
22. Wang XX, Pang ZY, Tong H, et al. (2019) Theoretical investigation of subwavelength structures fabrication based on multiexposure surface plasmon interference lithography. Results in Physics 12: 732-737.
23. Wang XX, Tong H, Pang ZY, et al. (2019) Theoretical realization of three-dimensional nanolattice structure fabrication based on high-order waveguide-mode interference and sample rotation. Optical and Quantum Electronics 51: 38.
24. Liang CP, Niu G, Chen XF, et al. (2019) Tunable triple-band graphene refractive index sensor with good angle-polarization tolerance. Optics Communications 436: 57-62.
25. Liu C, Su WQ, Liu Q, et al. (2018) Symmetrical dual D-shape photonic crystal fibers for surface plasmon resonance sensing. Optics Express 26(7): 9039-9049.
26. Liu ZQ, Yu MD, Huang S, et al. (2015) Enhancing refractive index sensing capability with hybrid plasmonic-photonic absorbers. Journal of Material Chemistry C 3: 4222-4226.
27. Qi YP, Zhang XW, Zhou PY, et al. (2018) Refractive index sensor and filter of metal-insulator-metal waveguide based on ring resonator embedded by cross structure. Acta Physica Sinica 67(19): 197301.
28. Cen CL, Lin H, Huang J, et al. (2018) A tunable plasmonic refractive index sensor with nanoring-strip graphene arrays. Sensors 18(12): 4489.
29. Liu C, Lin Y, Lu XL, et al. (2017) Mid-infrared surface plasmon resonance sensor based on photonic crystal fibers. Optics Express 25(13): 14227-14237.
30. Abutoama M, Abdulhalim I (2015) Self-referenced biosensor based on thin dielectric grating combined with thin metal film. Optics Express 23: 28667-28682.
31. Abutoama M, Abdulhalim I (2017) Angular and intensity modes self-referenced refractive index sensor based on thin dielectric grating combined with thin metal film. IEEE Journal of Selected Topics in Quantum Elctronics 23: 4600309.
32. Zhan GZ, Liang RS, Liang HT, et al. (2014) Asymmetric band-pass plasmonic nanodisk filter with mode inhibition and spectrally splitting capabilities. Optics Express 22: 9912-9919.
33. Lu H, Liu XM, Mao D (2012) Plasmonic analog of electromagnetically induced transparency in multi-nanoresonator-coupled waveguide systems. Physical Review A 85(5): 053803.

34. Wei W, Zhang X, Ren XM (2015) Plasmonic circular resonators for refractive index sensors and filters. Nanoscale Research Letters 10: 211.
35. Zou SW, Wang FQ, Liang RS, et al. (2015) A nanoscale refractive index sensor based on asymmetric plasmonic waveguide with a ring resonator: A review. IEEE Sensors Journal 15(2): 646-650.
36. Zhang HY, Shen DL, Zhang YP (2014) Circular split-ring core resonators used in nanoscale metal-insulator-metal band-stop filters. Laser Physics Letter 11(11): 115902.
37. Xie YY, Huang YX, Zhao WL, et al. (2015) A novel plasmonic sensor based on metal-insulator-metal waveguide with side-coupled hexagonal cavity. IEEE Photonics Journal 7(2): 4800612.
38. Bahramipanah M, Abrishamian MS, Mirtaheri SA, et al. (2014) Ultracompact plasmonic loop-stub notch filter and sensor. Sensors and Actuators B: Chemical 194: 311-318.
39. Maier SA (2007) Plasmonics: Fundamentals and Applications. Springer, USA.
40. Susan C Hagness (2005) Computational electrodynamics: The finite-difference time-domain method. Taflove A (Eds.).